From spherical expanding flames to laminar burning properties: a step-by-step analysis

Vincenzo Moccia[1,*], Jacopo D'Alessio[1], Natale Rispoli[2]

[1]Istituto Motori – C.N.R., Napoli, Italy
[2]Istituto di Fisica del Plasma – C.N.R., Milano, Italy
*corresponding author: v.moccia@im.cnr.it

Abstract The analysis is proposed of the process of deriving laminar burning parameters from high-speed, high resolution shadowgraph recording of spherical expanding flames. Data processing and analysis are critically discussed, starting from the extraction of flame radius from the experimental recordings.
A specific test case is used as a reference: CH_4-air mixtures have been tested in the high-pressure DHARMA reactor, at starting pressure of 6 bar and ambient temperature, varying the equivalence ratio within the flammability range.
Even in a simplified configuration, real flames are anyway affected by stretch: the critical point is processing the measured data to obtain the unstretched flame speed and, ultimately, the laminar burning velocity. A linear relationship is usually assumed between flame speed and stretch. In recent years, non-linear methodologies have been proposed as a more accurate approach to the deconvolution of experimental, stretch-affected data.
The comparison has been drawn in terms of unstretched laminar burning velocity and burned-gas Markstein length: the results have been referred to available literature. An overall picture of the applicability of the various options has been obtained, together with an estimate of each method's accuracy and of the associated errors (either physical or mathematical in nature).
Keywords: laminar burning velocity, Markstein length, shadowgraph, methane

1 Introduction

Ever since CO_2 reduction attained the status of main driver for energy technology development, a number of strategies have been pursued: from the promotion of CO_2-neutral fuels, to higher combustion efficiency (lower fuel consumption), to the use of low-carbon fuels (low C/H ratio). The practical accomplishment of these technology trends translates in the replacement of fossil fuels by biomass/renewable sources, in the retrofitting/design of combustion systems based on more efficient technologies, or, typically, in the combination of both approaches.
After the Hydrogen craze at the beginning of the century, the efforts to legitimate the scenario of H_2-based economy faded against a series of technological issues: the limitations were (and still are) related both to the large-scale H_2 production and to the cost-effective mass-production of end-user systems. In this respect, methane (CH_4, the main constituent of Natural Gas) has been revamped as the hydrocarbon fuel of choice: it suits several energy conversion systems and, moreover, its "performance" can be easily enhanced by means of H_2 addition. Apart from CH_4, in recent years a wide range of fuels has been steadily proposed, deriving from the gasification of biomass, wastes and even fossil fuels: the technological appeal of fuels like *syngas* or *biogas* resides in the potential of CO_2-neutral energy conversion, of waste recycling, of small scale CHP production. The composition of these gas fuels is strongly affected by the production process and by the feedstock.
Therefore the picture emerges of a wide range of eco-friendly gas mixtures, which are asking for characterization as fuels. In order to optimize and/or design i.c. engines and gas turbine combustors, the knowledge is needed of the fuel-specific combustion properties: these can be expressed in terms of laminar burning velocity and Markstein length, and offer the basis for modelling and simulation of flame-turbulence interaction.
Even if object of intensive research activity in the last 50 years [1][2][3][4][5][6][7][8][9], the accurate determination of these parameters is still a matter of debate. Spherical expanding flames offer a number of advantages: they allow high-pressure testing and are conceptually simple to analyze. Nevertheless, what can appear as a straightforward approach is actually a delicate evaluation process, punctuated by subtle pitfalls: failing to realize this may lead to less than accurate results. Many authors focused on the effects of ignition [4][10], radiation and buoyancy [11], confinement and chamber geometry [12], not to mention

instability[13]. Yet the core of the process leading from the experimental data to the laminar parameters (u_{l0} and L_b) is the stretch analysis. If the laminar burning velocity is the ideal speed at which a planar flame front propagates normally to its surface, the flame speed in real system is affected by stretch: the latter is the temporal flame surface deformation, which condition the propagation, stability and structure of the flame. Evaluating the functional relation between flame speed and stretch remains the big challenge in the quest for accurate laminar burning properties.

2 Experimental Layout and Procedures

The general arrangement of the experimental layout is shown in Figure 1: a detailed description is given in [14]. The heart of the DHARMA (*Device for Hydrogen-Air Reaction Mode Analysis*) laboratory is a constant-volume test reactor, made of stainless steel (AISI 316): the cylindrical chamber (i.d. = 70 mm, h = 90 mm, aspect ratio = 1.29) is rated for maximum pressure $\leq$ 20 MPa (static).
A total of 6 optical accesses are available: the larger viewports (d = 65 mm) are located normal to the chamber axis, providing nearly full access to chamber bore; smaller diameter ports are positioned on the chamber side, along two orthogonal axes. Hi-grade quartz windows (85 mm diameter, 30 mm thick) are installed in the main ports, the smaller side ports can be fitted either with quartz windows (49 mm diameter, 20 mm thick) or with a variety of stainless steel adapters (i.e., transducers, electrodes, sampling ports, etc.).
Four additional service ports are available, e.g., for the intake of the combusting mixture and the vent of the exhaust gases.
The mixture is ignited with an automotive inductive ignition system (energy $\leq$ 60 mJ), which was characterized recording the time evolution of the voltage drop and the current flow between the electrodes: this allowed to evaluate the power and energy release. Being known the electrical behavior of the coil, the energy of discharge can be set in the range 0÷60 mJ, adjusting the time of charge (dwell time). The spark discharge takes place in the center of the chamber between two pointed-tip tungsten electrodes (dia. = 1 mm, gap = 1 mm).

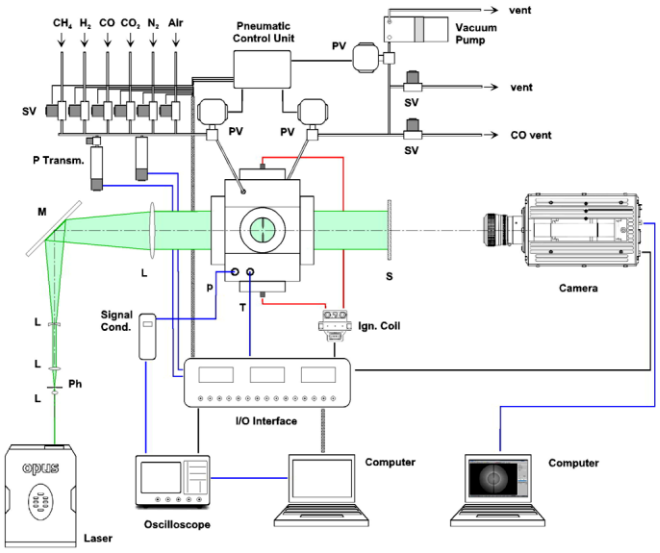

Fig. 1 Layout of the experimental apparatus

A high-frequency dynamic pressure transducer detects pressure history during the combustion events. A metal-shielded, type K thermocouple is used to monitor the temperature of the gases, save for the combustion phase.
The gas handling system was designed to prepare combustible mixtures of variable composition with high accuracy, spanning a range of initial pressures, which included values of relevance in spark-ignition engine operation.
High purity gases (CH_4: 99.9995%, H_2: 99.999%, CO: 99,999%, CO_2: 99,998%, N_2: 99.9995%, dry air: 99.999%) are used to prepare the mixtures, relying on the partial pressures method: the amount of each gas is

metered by a solenoid valve, controlled by a high-resolution (100 MHz) counter/timer board installed in the main computer. The pressure is monitored by two high-accuracy (±0.08% FS) pressure transmitters, operating in the range 0-1 bar and 0–30 bar. The gas supply system allows one to prepare combustible mixtures up to 30 bar. After each test, the system is vented, purged with N_2 and pumped down to 10^{-2} mbar. All the devices operate with a high degree of automation, to maximize safety and repeatability of the tests.
The entire lab conforms to current safety standards on the use of combustible gases, and is provided with interconnected gas leak sensors, cylinder cut-off devices and forced venting systems.

2.1 Optical Setup

A parallel-beam direct shadowgraph layout was set up, based on state-of-the-art devices and highly optimized optic arrangement. A Diode-Pumped Solid-State c.w. laser (Laser Quantum mod. Opus 2W @532nm) is used as the light source, offering plenty of light power, compact size factor, good power stability (0.4% rms) and excellent beam characteristics, including low divergence (0.4 mrad). The whole optical setup is arranged on an optical bench: laser beam is first expanded and spatially filtered by means of a Keplerian beam expander. A second expansion is obtained with a couple of lenses arranged in a Galilean configuration: the resulting beam size is 72 mm, exceeding the reactor viewport diameter (65 mm). Shadowgraphs are collected on a 220 grit translucent screen. High-speed, time-resolved visualization is accomplished by means of a CMOS camera (Photron mod. SA-5), which meets a series of critical requirements for the analysis of flame front propagation: high spatial resolution (1024x1024 pixel), 12 bit A/D converter, high framing rate (up to 1000000 fps) and short shutter time (≥ 368 ns). Shadowgraphs are imaged through a Nikon 60 mm f/2.8D AF Micro, characterized by a very low spatial image distortion.

2.2 Image processing

An image processing routine has been implemented to infer the flame radius r_u from the shadowgraph data. Assuming the luminous front in the shadowgraph corresponds to the radius on the unburned gas side [15] [16], for each frame the flame contour is traced and the area of the projected flame ball is evaluated; the radius is estimated as that of a circle of equal area to the flame. The time evolution of the *unburned* flame radius r_u offers the basis for the evaluation of the laminar parameters (u_{l0} and L_b).

3 Theoretical analysis

The stretched flame speed V_s is defined as:

$$V_s = \frac{dr_u}{dt} \tag{1}$$

The obtained speed includes the stretch effects associated to the propagation of a flame surface, which experiences curvature and flow dynamic strain [17][18][19][20]. The flame stretch α is defined as the relative rate of change of the flame area: for a spherically expanding laminar flame; it can be expressed as:

$$\alpha = \frac{1}{A}\frac{dA}{dt} = \frac{2}{r_u}\frac{dr_u}{dt} = 2\frac{V_s}{r_u} \tag{2}$$

The relationship between flame speed and stretch has been thoroughly investigated: its expression depends on the number and nature of the related assumptions. Historically, a linear formulation has been suggested[17][20]: it derives from asymptotic analysis and has found wide application. It can be expressed in a dimensional form, suitable for data reduction, as follows:

$$V_s = V_{s0} - L_b \cdot \alpha \tag{3}$$

where V_{s0} is the value assumed by V_s at α = 0, and L_b is the *burned gas* Markstein length. The latter indicates

how and to what extent the flame is influenced by the stretch. Positive L_b are associated to flames with speed decreasing with stretch (which are stable), while in the case of negative L_b the flame speed tends to increase with stretch, becoming unstable; moreover, the magnitude of L_b indicates to what extent the flame propagation is influenced by the stretch.

Back in 1983, Frankel and Sivashinsky [21] suggested the following equation for spherical flames with thermal expansion:

$$V_s = V_{s0} - V_{s0} L_b \cdot \frac{2}{r_u} \tag{4}$$

where V_s is given by Eq. (1). According to Eq. (4), V_s varies linearly with flame curvature $2/r_u$.

Equation (3) shows a *linear* relationship between V_s and the stretch rate α. It is obtained assuming a small deviation of the flame speed from a planar, adiabatic value. In a more general case (no small stretch, density variation, adiabatic and quasi-steady flame), the propagation speed can be expressed as [22][23]:

$$\left(\frac{V_s}{V_{s0}}\right)^2 \ln\left(\frac{V_s}{V_{s0}}\right)^2 = -\frac{2L_b\alpha}{V_{s0}} \tag{5}$$

The models given by Equations (3) (4) and (5) can be used to extract the unstretched laminar flame speed and Markstein length from spherical expanding flames. These models can be classified on the basis of the relationship between V_s and α: in this framework, Eq. (3) will be referred to as "linear model", while Eq. (4) and (5) as "nonlinear models".
Once evaluated the flame speed V_{s0}, the laminar burning velocity u_{l0} can be obtained as follows:

$$u_{l0} = V_{s0} \frac{\rho_b}{\rho_u} \tag{6}$$

where ρ_b is the density of burned gases and ρ_u the density of unburned gases. Equation (6) holds true in the hypotheses of perfect gases, isobaric, adiabatic and equilibrium conditions
In the following the comparison is proposed and discussed between the linear and nonlinear approaches to data analysis (reduction). Two different methods are evaluated to solve the linear Equation (3); the solutions of nonlinear Equations (4) and (5), as suggested in literature, are tested also in terms of mathematical stiffness. The comparison is carried out with reference to the test case of CH_4-air mixture at T_0 = 298 K, P_0 = 6 bar, the equivalence ratio ϕ varying between the flammability limits (0.6 ÷ 1.6).

4 Data processing

4.1 Linear models

The long-established approach for the linear analysis consists of a series of steps: a polynomial fit of $r_u = r_u(t)$ is first performed; differentiation of the fit allows to obtain the stretched flame speed V_s after Eq. (1); being known V_s and r_u, the stretch rate α can be evaluated after Eq. (2); according to Eq. (3), linear-fit extrapolation of the flame speed to α = 0 gives the unstretched flame speed V_{s0}, while the slope of the fit allows to estimate the Markstein length L_b. The critical issue in this methodology resides in the polynomial differentiation, which is highly sensitive to the choice of the original data interval: this may introduce numerical noise and lead to distorted profiles of V_s, affecting both V_{s0} and L_b.

4.1.1 Linear Model I

In 2007 Burluka *et al*. [24] suggested an analytical procedure to infer V_{s0} and L_b directly from the temporal evolution of the flame radius. Substitution of Eq. (2) into Eq. (3) gives, after integration:

$$r_u(t) - r_u(t_0) + 2L_b \cdot \ln\left(\frac{r_u(t)}{r_u(t_0)}\right) = V_s(t - t_0) \tag{7}$$

The problem reduces to the optimization of the least square function:

$$\Psi(L_b, V_{s0}) = \sum_{i=1}^{N}\left(t_i - t_0 - \frac{r_i - r_0}{V_{s0}} - 2 \cdot \frac{L_b}{V_{s0}} \cdot \ln\left(\frac{r_i}{r_0}\right)\right)^2 \tag{8}$$

This is easily implemented, no data differentiation is performed, and no singularity is present (the case of L_b=0 is allowed). The critical point of this approach lies in the selection of the initial conditions (t_0 and r_0). In order to circumvent this issue, we modified the procedure, performing N estimates (N = no. of data points), choosing each time a different value of r_0 from the available set. The final values of V_{s0} and L_b are then obtained as the average of the N values of V_{s0} and L_b evaluated as described above.
Even with a large number of data points (t, r_u), the method demonstrated to be fast and robust.

4.1.2 Linear Model II

In 2009 Tahtouh *et al*. [16] suggested an elegant analytical methodology which offers the exact solution of the linear Equation (3). Equations (2) and (3) can be rearranged as follows:

$$\frac{dr}{dt} = V_{s0} - 2L_b \cdot \frac{dr}{rdt} \tag{9}$$

The solution of Equation (9) is:

$$r(t) = 2L_b W(Z) \tag{10}$$

Where W is the Lambert function, and Z is given by:

$$Z = \frac{e^{\frac{V_{s0}t + C_1}{2L_b}}}{2L_b} \tag{11}$$

Where C_1 is a constant to be determined. The values of V_{s0} and L_b (and C_1) are obtained minimizing the following Equation:

$$\sum_{1}^{N}\left(r_u(t) - r(t)\right)^2 = \sum_{1}^{N}\left(r_u(t) - 2L_b W(Z)\right)^2 \tag{12}$$

where r_u is the experimentally measured radius. The Lambert function W is a multi-valued function [25]: if Z is real, for $-1/e \le Z < 0$ $W(Z)$ can assume two possible real values. The branch satisfying the condition $-1 \le W(Z)$ is termed the *principal* branch and denoted $W_0(Z)$. The branch satisfying the condition $W(Z) \le -1$ is called the *alternate* branch and denoted $W_{-1}(Z)$. For $L_b > 0$ (that is $Z > 0$), the principal branch of the Lambert function (W_0) must be used, while for $L_b < 0$, $W_{-1}(Z)$ should be used. This method delivers directly V_{s0} and L_b for each test case, no differentiation is needed and all the data are used simultaneously, with the same weight.
The major drawback is that the function is not defined for L_b=0: a preliminary guess is needed on the sign of L_b, in order to use the principal $W_0(Z)$ or the alternate branch $W_{-1}(Z)$ of the Lambert function. An independent *a priori* estimate of the sign of L_b is therefore needed, to be performed with a different method.

Moreover, when L_b has very small absolute value, the model may become unstable: if the preliminary estimate suggest a value with the wrong sign, the wrong branch of the Lambert function will be selected and the method will fail to converge.

4.2 Nonlinear models

4.2.1 Nonlinear Model I

Substitution of Eq. (1) into Eq. (4) gives:

$$\frac{dr_u}{dt} = V_{s0} - V_{s0} L_b \cdot \frac{2}{r_u} \tag{13}$$

This equation can be analytically solved and the values of V_{s0} and L_b can be obtained by a nonlinear least-square method, without the need of numerical differentiation. This is a simple and robust formulation, offering the best compromise between accuracy and reliability.

4.2.2 Nonlinear Model II

In 2007 Kelley & Law [26] suggested an analytical solution of Equation (5), allowing to obtain directly V_{s0} and L_b from the raw data of flame radius as a function of time r_u(t).
Integration of Eq. (2) gives:

$$t = A\left[E_1(\ln \tau^2) - \frac{1}{\tau^2 \ln \tau} \right] + C \tag{14}$$

where

$$A = \frac{2L_b}{V_{s0}}, \qquad r_u = \frac{2L_b}{\tau \ln \tau}, \qquad E_1(x) = \int_x^\infty \frac{e^{-z}}{z} dz \tag{15}$$

Equation (14) is suitable for nonlinear least-square regression, allowing A, L_b and C to be determined.
$\tau \in [1/e, 1]$ for $L_b > 0$ and $\tau \in [1, \infty]$ for $L_b < 0$.
In the present work, we replaced the expression for E_1 with the following:

$$E_1(x) = \ln\left|\frac{x}{2}\right| + \sum_{k=1}^{\infty} (-1)^k \frac{x^k}{k \cdot k!} \tag{16}$$

which results always defined in a real domain, even for $\tau \in [1/e, 1]$.
The model has the unquestionable advantage of offering an explicit analytical solution, and handles well the cases of nonlinear behavior of V_s vs. α.
Nevertheless, the expression asks for some care. The transformed time variable has different spacing from the original data set: at every step, the outputs from the algorithm have to be interpolated in order to be compared with the input data. This may be a source of interpolation noise (error). Even if the case of $L_b = 0$ offers no problem, a preliminary estimate of the starting values will improve the convergence of the solver. The region $\tau \in [1/e, e]$ can be tricky for the model to handle.

Table 1 summarizes the above-described models.

Table 1 – Summary of the tested models

author(s)	*type of model*	*solution*	*short form*
Burluka *et al.* (2007)	linear	explicit	LM I
Tahtouh *et al.* (2009)	linear	through least-square	LM II
Frankel & Sivashinsky (1983)	nonlinear	through least-square	NM I
Kelley & Law (2007)	nonlinear	through least-square	NM II

5 Results

In the following the four methods for the extraction of laminar burning properties are compared against the test case of CH_4–air combustion at 6 bar and 298 K, varying the equivalence ratio ϕ.
The raw data consist of the time evolution of the flame radius $r_u = r_u(t)$, as inferred from high-speed shadowgraph recordings of spherical expanding flames.
Figure 2 shows $r_u = r_u(t)$ for lean and rich mixtures. A few conditions have to be satisfied for the correct evaluation of laminar flame properties: the analysis must be carried out only in the constant-pressure phase, before the chamber pressure shows a sensible increment: this defines the upper bound of the valid data subset. Moreover, as stated by Bradley *et al.* [4], the early stages of the flame kernel growth are affected by the spark energy release, and must be discarded: this defines the lower bound of the data set.
In the present tests, spark energy was set at 20 mJ (electrical). Given the small spark energy, the extent of the ignition disturbances can be expected to be accordingly limited.
Analysis of the flame radii in the early stages revealed no discernible evidence of ignition-induced effects: nonetheless, pending further investigation, a conservative criterion was applied, based on the morphology of the flame: flames with an aspect ratio (major axis/minor axis of the fitting ellipse) lower than 0.98 were discarded. Typical value for the minimum radius was about 4 mm.

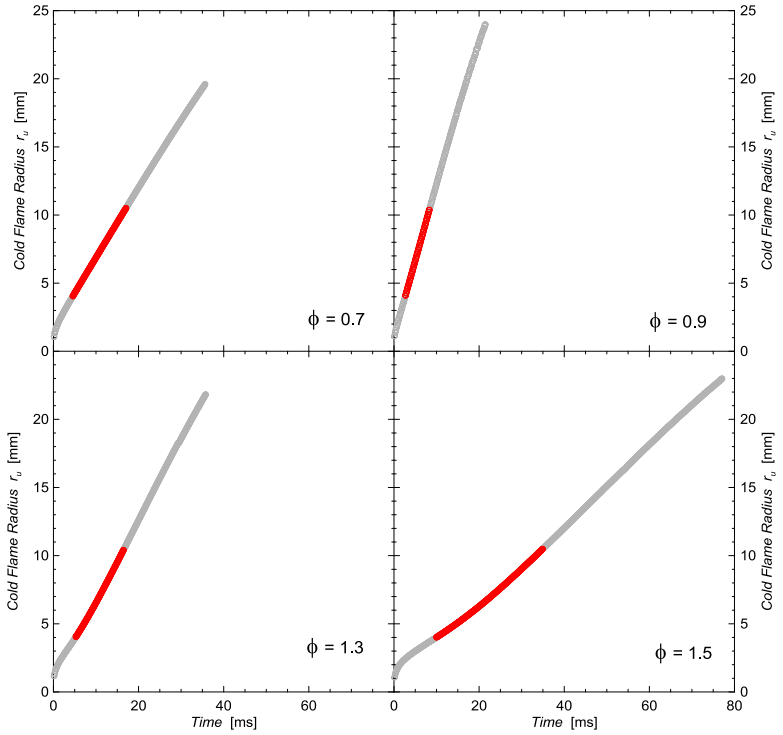

Fig. 2 Time evolution of flame radius for CH_4-air mixtures at different ϕ. $T_0 = 298$ K, $P_0 = 6$ bar.

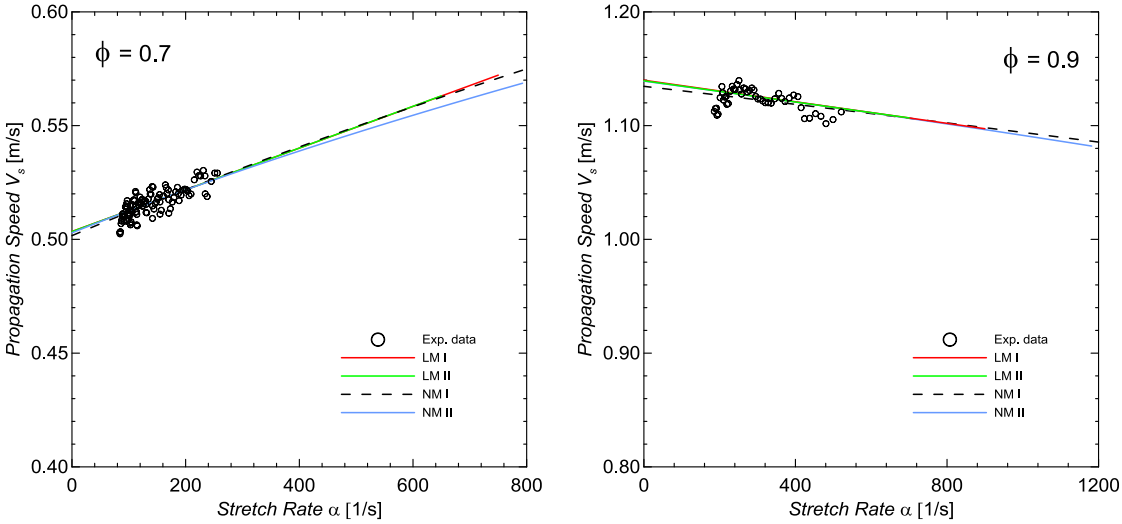

Fig. 3 Comparison of linear and nonlinear models for lean CH_4-air mixtures. T_0 = 298 K, P_0 = 6 bar.

As stated above, the maximum radius was obtained applying the constraint of constant pressure: typical value was ~10 mm, corresponding to ~29% of the chamber radius. This value meets the ($r_u < 0.3r_{chamber}$) criterion suggested by Burke *et al*. [12] to avoid the effects of confinement in a cylindrical chamber. The useful data interval, defined with the criteria described above, is evidenced with red symbols in Fig. 2 for each case.

In Fig. 3 the comparison is proposed between the different models, along with the experimental data. Two lean mixtures (ϕ = 0.7 and 0.9) are shown, highlighting an almost linear variation of the propagation speed as a function of the stretch rate. LM I and LM II deliver virtually the same values for V_{s0} and L_b, which are very close to the results obtained with either NM I or NM II. Actually, at ϕ = 0.7 and ϕ = 0.9 the Markstein length is very close to 0, standing for a modest sensitivity of flame speed on stretch: a linear models can be meaningfully applied and offers accurate results.

Figure 4 shows two examples of rich mixtures (ϕ = 1.3 and 1.5): as the equivalence ratio increases, the relationship between the propagation speed and the stretch keeps deviating from linearity. The difference between LM I (or LM II) and the nonlinear models indicates that a linear model is no more valid: as a matter of fact, Markstein lengths are much larger (by an order of magnitude), corresponding to regimes of flame evolution much more sensitive to stretch. In these conditions, application of either LM I or LM II leads to overestimation of L_b and consequently of V_{s0}. Comparison of NM I and NM II reveals that the experimental data are typically better fitted by the former model: NM II tends to underestimate either the Markstein length or the unstretched flame speed.

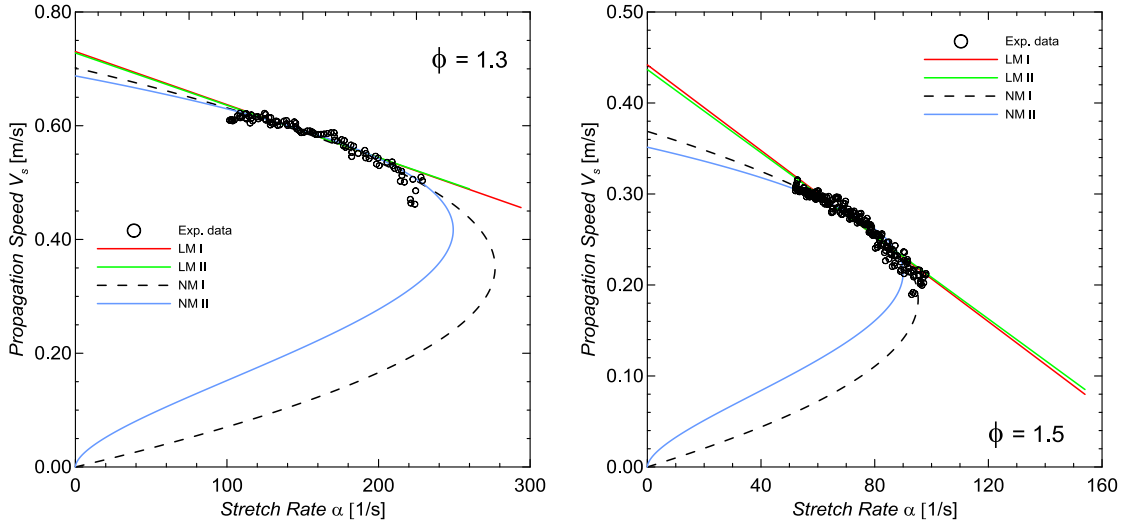

Fig. 4 Comparison of linear and nonlinear models for rich CH_4-air mixtures . T_0 = 298 K, P_0 = 6 bar.

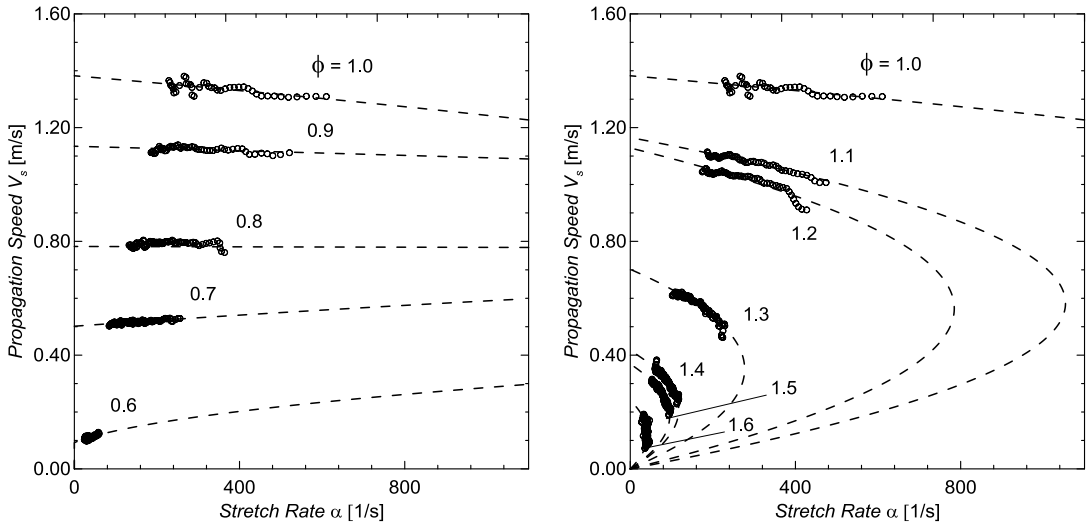

Fig. 5 Evolution of stretched flame speed with stretch for lean and rich mixtures. T_0 = 298 K, P_0 = 6 bar.

Figure 5 shows the overall behavior of V_s vs. α, within the whole flammability interval. As anticipated by the examples discussed above, CH_4-air mixtures exhibit stronger nonlinearity as the equivalence ratio is increased. These results are in perfect agreement with the findings of Halter *et al.*, obtained with the same mixture at ambient temperature and pressure [23]. The dashed lines represent the results obtained with NM I, which effectively and accurately describe the flame-stretch interaction, whatever the equivalence ratio.
The burned gas Markstein length and the laminar burning velocity, evaluated after Eq. (6), are shown in Fig. 6. The graphs include the results for the various models, LM I, LM II, NM I and NM II, allowing for an immediate comparison of their validity and accuracy. As remarked above, the Markstein length increases with the equivalence ratio: it's negative for very lean mixtures and changes sign at ϕ = 0.8 ÷ 0.9.
For equivalence ratios ϕ ≤ 1.2, $|L_b|$ < 0.5 mm and the dependence of the flame speed on stretch can be considered linear with good approximation. For ϕ > 1.2, this relationship becomes nonlinear: as a consequence, linear models tend to overestimate L_b and, in turn, the unstretched flame speed.
This ultimately leads to overestimation of the laminar burning velocity, as indicated in Fig. 6 (right): the values of u_{l0} obtained with linear and nonlinear models are virtually coincident up to ϕ = 1.2, but for richer mixtures an increasing difference is noted between LM's and NM's.

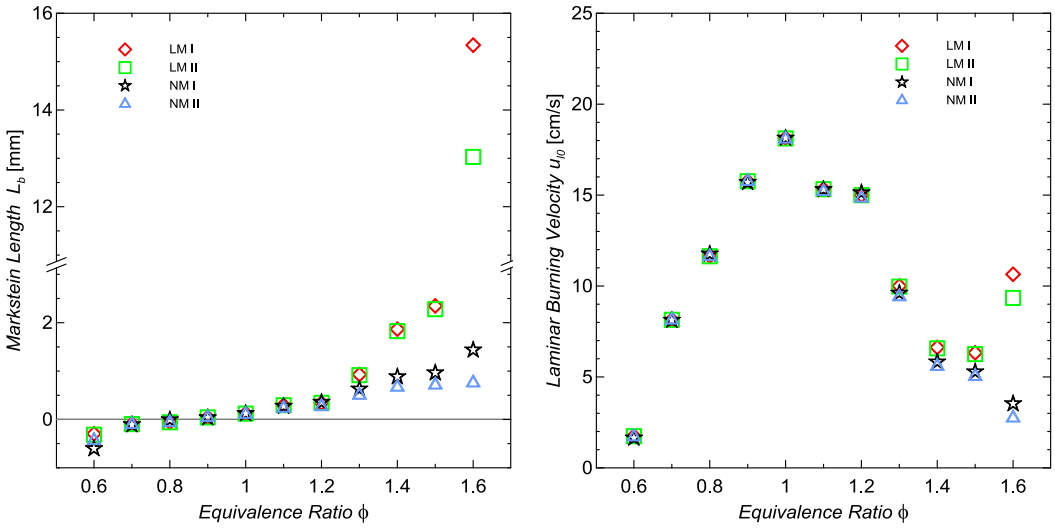

Fig. 6 Markstein length (left) and Laminar Burning Velocity (right) as obtained by different models. CH_4-air, T_0 = 298 K, P_0 = 6 bar.

These results are represented in Fig. 7 in terms of relative differences: assuming NM I as the reference, the

error induced by the use of the other models can be defined as:

$$\varepsilon_i = \frac{u_{l0}^{i} - u_{l0}^{NMI}}{u_{l0}^{NMI}} \tag{17}$$

where u_{l0}^{NMI} is the laminar burning velocity evaluated with NM I, and u_{l0}^{i} the velocity obtained with model i (i = LM I, LM II, NM II). Apart from the case of $\phi = 0.6$, where higher relative errors can be expected, due to the low absolute value of the velocity involved, ε_i keeps limited to a few percent up to $\phi = 1.2$, then for LM I and LM II exponentially increases, reaching ~20% at $\phi = 1.5$. Errors as high as 200%, obtained with LM I at the rich flammability limit ($\phi = 1.6$), stand for the definite inaccuracy of linear models for rich CH_4-air mixtures. While both linear models tend to overestimate the laminar burning velocity, the method suggested by Kelley & Law (NM II) leans towards underestimation, even if the absolute value of ε_i does not exceed 5% for $\phi \leq 1.5$.
These findings confirm the conclusions of Chen [27], who carried out an in-depth comparison of linear and nonlinear models against both simulated data and experimental results. He concluded that NM I is the most accurate model for analyzing data with positive Markstein length, which is the case for most of the methane-air mixtures within the flammability interval.

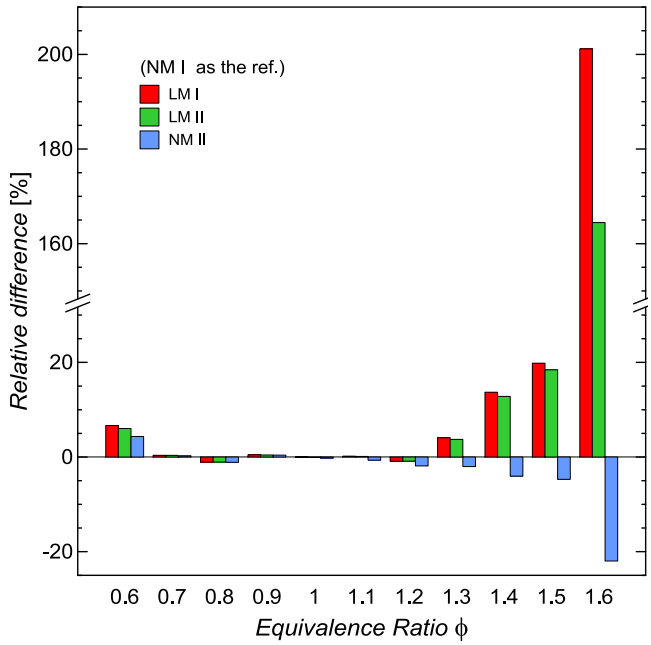

Fig. 7 Relative difference in laminar burning velocity between the tested models, with reference to NM I. CH_4-air, T_0 = 298 K, P_0 = 6 bar.

Conclusions

Four methodologies have been compared for the deconvolution of flame speed (in constant-pressure spherical expanding flames) from the stretch: LM I and LM II were based on the hypothesis of a linear dependence of V_s on α; NM I and NM II were based on a more complex, nonlinear relation.
In order to identify the most correct approach to stretch analysis, and to infer accurate values of the laminar parameters, the study was aimed to assess the limits of application for the simpler linear models, and the associated error. The comparison was carried out against two nonlinear models proposed in literature.
All the tested models offer the appeal of an analytical solution, allowing to infer V_{s0} and L_b directly from the experimental data, without the need for numerical differentiation of the raw data.
CH_4-air mixtures (T_0=298 K, P_0=6 bar, $\phi_{min} < \phi < \phi_{max}$) were used as the reference case.

The main findings can be summarized as follows:

- NM I demonstrated to be the most accurate model in the case of methane, which is characterized by a positive Markstein length in nearly all the flammability interval (corresponding to $Le > Le^*$)
- For $\phi \leq 1.2$, CH_4 exhibits a linear behaviour of V_s vs. α: this implies LM I and LM II can be meaningfully applied up to this value of the equivalence ratio
- For $\phi > 1.2$, the evolution of the propagation speed cannot be considered linear, and the application of either LM I or LM II gives rise to growing errors in the estimate of V_{s0} and L_b
- Incorrect application of linear models can lead to errors on the laminar burning velocity as high as 20% ($\phi = 1.5$) or even larger (150÷200% at $\phi = 1.6$).

Acknowledgments

The research was partially supported by the Italian Ministry of Economic Development within the framework of the Program Agreement MiSE-CNR "Ricerca di Sistema Elettrico".

References

[1] Lewis B, von Elbe G (1934) Determination of the speed of flames and the temperature distribution in a spherical bomb from time-pressure explosion records. *J. Chem. Phys.* Vol. 2, pp 283–290. doi:10.1063/1.1749464

[2] Milton B E, Keck J C (1984) Laminar burning velocities in stoichiometric hydrogen and hydrogen-hydrocarbon gas mixtures. *Combustion and Flame*, vol. 58, pp 13–22. doi: 10.1016/0010-2180(84)90074-9

[3] Egolfopoulos F N, Cho P, Law C K (1989) Laminar flame speeds of methane-air mixtures under reduced and elevated pressures. *Combustion and Flame*, vol. 76, pp 375–391. doi: 10.1016/0010-2180(89)90119-3

[4] Bradley D, Gaskell P H, Gu X J (1996) Burning velocities, markstein lengths, and flame quenching for spherical methane-air flames: A computational study. *Combustion and Flame*, vol. 104, pp 176–198. doi: 10.1016/S0010-2180(99)00142-X

[5] Hassan M I, Aung K T, Faeth G M (1998) Measured and Predicted Properties of Laminar Premixed Methane/Air Flames at Various Pressures. *Combustion and Flame*, vol. 115, pp 539-550. doi: 10.1016/S0010-2180(98)00025-X

[6] Gu X J, Haq M Z, Lawes M, Woolley R (2000) Laminar burning velocity and markstein lengths of methane-air mixtures. *Combustion and Flame*, vol. 121, pp 41–58. doi: 10.1016/S0010-2180(99)00142-X

[7] Rozenchan G, Zhu D L, Law C K, Tse S D (2002) Outward propagation, burning velocities, and chemical effects of methane flames up to 60 atm. *Proceeding of the Combustion Institute*, vol. 29, pp 1461-1469. doi: 10.1016/S1540-7489(02)80179-1

[8] Halter F, Chauveau C, Djebaili-Chaumeix N, Gokalp I (2005) Characterization of the effects of pressure and hydrogen concentration on laminar burning velocities of methane-hydrogen-air mixtures. *Proceeding of the Combustion Institute*, vol. 30, pp 201-208. doi: 10.1016/j.proci.2004.08.195

[9] Huang Z, Zhang Y, Zeng K, Liu B, Wang Q, Jiang D (2006) Measurements of laminar burning velocities for natural gas-hydrogen-air mixtures. *Combustion and Flame*, vol. 146, pp 302-311. doi: 10.1016/j.combustflame.2006.03.003

[10] Chen Z, Burke M P, Ju Y (2009) Effects of Lewis number and ignition energy on the determination of laminar flame speed using propagating spherical flames. *Proceeding of the Combustion Institute*, vol. 32, pp 1253-1260. doi: 10.1016/j.proci.2008.05.060

[11] Chen Z, Qin X, Xu B, Ju Y G, Liu F S (2007) Studies of radiation absorption on flame speed and flammability limit of CO2 diluted methane flames at elevated pressures. *Proceeding of the Combustion*

Institute, vol. 31, pp 2693-2700. doi: 10.1016/j.proci.2006.07.202

[12] Burke M P, Chen Z, Ju Y, Dryer F L (2009) Effect of cylindrical confinement on the determination of laminar flame speeds using outwardly propagating flames. *Combustion and Flame*, vol. 156, pp 771-779. doi: 10.1016/j.combustflame.2009.01.013

[13] Bradley D, Harper C M (1994) The development of instabilities in laminar explosion flames. *Combustion and Flame*, vol. 99, pp 562–572. doi: 10.1016/0010-2180(94)90049-3

[14] Moccia V, D'Alessio J (2011) Evaluating the Burning Velocity of Gaseous Fuels for Engine Applications: the DHARMA Project. *SAE Technical Paper*, 2011-24-0056. doi: 10.4271/2011-24-0056

[15] Parsinejad F, Keck J, Metghalchi H (2007) On the location of flame edge in Shadowgraph pictures of spherical flames: a theoretical and experimental study. *Exeriments in Fluids*, vol. 43, pp 887-894. doi: 10.1007/s00348-007-0355-6

[16] Tahtouh T, Halter F, Mounaïm-Rousselle C (2009) Measurement of laminar burning speeds and Markstein lengths using a novel methodology. *Combustion and Flame*, vol. 156, pp 1735–1743. doi: 10.1016/j.combustflame.2009.03.013

[17] Markstein G H (1951) Experimental and theoretical studies of flame-front stability. *Journal of Aeronautical Sciences*, vol. 18, pp 199-209. doi: 10.2514/8.1900

[18] Karlovitz B, Denniston Jr. D W, Knapschaefer D H, Wells F E (1953) Studies on Turbulent Flames: A. Flame Propagation Across Velocity Gradients, B. Turbulence Measurement in Flames. *Symposium (International) on Combustion*, vol. 4, pp 613-620. doi: 10.1016/S0082-0784(53)80082-2

[19] Matalon M (1983) On flame stretch. *Combustion Science and Technology*, vol. 31, pp 169–181. doi: 10.1080/00102208308923638

[20] Clavin P (1985) Dynamic Behavior of Premixed Flame Fronts in Laminar and Turbulent Flows. *Progress in Energy and Combustion Science*, vol. 11, pp 1–59. doi: 10.1016/0360-1285(85)90012-7

[21] Frankel M L, Sivashinsky G I (1983) On Effects Due To Thermal Expansion and Lewis Number in Spherical Flame Propagation. *Combustion Science and Technology*, vol. 31, pp 131–138. doi: 10.1080/00102208308923635

[22] Kelley A P, Law C K (2009) Nonlinear effects in the extraction of laminar flame speeds from expanding spherical flames *Combustion and Flame, vol.* 156, pp 1844-1851. doi: 10.1016/j.combustflame.2009.04.004

[23] Halter F, Tahtouh T, Mounaïm-Rousselle C (2010) Nonlinear effects of stretch on the flame front propagation. *Combustion and Flame*, vol. *157*, pp 1825–1832. doi: 10.1016/j.combustflame.2010.05.013

[24] Burluka A A, Fairweather M, Ormsby M B, Sheppard C G W, Wooley R (2007) The Laminar Burning Properties of Premixed Hydrogen-Air Flames Determined Using a Novel Analysis method. In: Proceedings of Third European Combustion Meeting (ECM 2007)

[25] Corless R M, Gonnet G H, Hare D E G, Jeffrey D J, Knuth D E (1996) On the Lambert W function. *Advances in Computational Mathematics*, vol 5, pp 329–359. doi: 10.1007/BF02124750

[26] Kelley A P, Law C K (2007) Nonlinear effects in the experimental determination of laminar flame properties from stretched flames. In: Proceeding of Eastern State Fall Technical Meeting, Chemical & Physical Processes in Combustion

[27] Chen Z (2011) On the extraction of laminar flame speed and Markstein length from outwardly propagating flames. *Combustion and Flame.* vol. 158, pp 291 – 300. doi: 10.1016/j.combustflame.2010.09.001